Neoclassical Currents and Transport Studies in HSX at 1 Tesla

J.N. Talmadge 1), D.T. Anderson 1), F.S.B. Anderson 1), C. Deng 2), W. Guttenfelder 3), K.M. Likin 1), J. Lore 1), J.C. Schmitt 1), K. Zhai 1)

1) HSX Plasma Laboratory, University of Wisconsin-Madison, Madison, WI, USA
2) University of California-Los Angeles, Los Angeles, CA, USA
3) University of Warwick, Coventry, United Kingdom

email contact of main author: talmadge@wisc.edu

Abstract. HSX is a quasihelically symmetric stellarator with minimal toroidal curvature and a high effective transform. Experimental measurements of neoclassical currents and transport studies at 1 Tesla operation are presented. An array of magnetic pickup coils placed at two toroidal locations demonstrates that the Pfirsch-Schlüter current is helical. Measurements of the poloidal component of the magnetic field show good agreement with calculations based on a combination of VMEC, BOOTSJ and the V3FIT code. Electron temperatures in the core during ECRH are up to 2.5 keV with 100 kW input power and drop to 1.5 keV when the symmetry is intentionally degraded and the neoclassical transport is increased. The steep temperature gradient in the core region is indicative of a CERC (core electron root confinement), often seen in conventional stellarators. Calculations using the PENTA code, which includes momentum conservation and parallel flows, indicate that the radial electric field for the quasihelical configuration is roughly half that obtained using the DKES code for the region of the plasma in the electron root. A Weiland ITG/TEM tokamak model for anomalous transport, which corrects for the local geometry in HSX, supports the conclusion that E×B suppression of turbulence is responsible for the improved confinement in the plasma core. The experimental confinement time scaling with power agrees well with the model.

1. Introduction

The Helically Symmetric Experiment (HSX) is of a class of stellarators in which the Fourier decomposition of |B| on a magnetic surface is dominated by a single harmonic. In such a configuration the large increase in transport at low collisionality typical of conventional stellarators is avoided. For a quasihelically symmetric (QHS) stellarator like HSX, the magnitude of the magnetic field can be written as

$$B/B_0 = 1 - b_{nm}\cos(n\varphi - m\theta), \tag{1}$$

where φ is the toroidal angle and θ is the poloidal angle. In a straight field-line coordinate system given by $\theta = \iota\varphi$, where ι is the rotational transform, the magnetic field variation on the field line is given by

$$B/B_0 = 1 - b_{nm}\cos([n - m\iota]\varphi). \tag{2}$$

Substituting $\iota_{eff} = n - m\iota$ for the rotational transform, the variation of |B| is the same as in a tokamak. For HSX, with $n = 4$, $m = 1$ and $\iota \geq 1$, the effective transform ι_{eff} is about 3. Compared to a tokamak with the same real transform ι, the high effective transform in HSX results in smaller: drifts of passing particles from a flux surface, banana orbits, neoclassical transport, as well as lower Pfirsch-Schlüter and bootstrap currents.

In addition to the 48 nonplanar modular coils that produce the quasihelical field, there is a set of 48 planar auxiliary coils which can add additional Fourier harmonics [n,m] = [4,0] and [8,0] to the magnetic field spectrum. Neoclassical transport in this configuration, termed Mirror, is increased back to the level of a conventional stellarator, while the plasma volume, rotational transform and magnetic well depth vary little from the QHS configuration.

Plasmas in HSX are formed and heated using a 28 GHz gyrotron to launch the fundamental ordinary mode at 1 Tesla. Plasma densities are limited by the electron cyclotron resonant heating (ECRH) cut-off to 1×10^{13} cm^{-3} and maximum input power is 100 kW. Electron transport in the low collisionality regime can be studied by varying the magnetic field spectrum with the auxiliary coils. Previous experiments at 0.5 Tesla reported a superthermal electron population that complicated the determination of the absorbed power [1]. At 1.0 Tesla the superthermal population is greatly reduced based on diamagnetic, electron cyclotron emission and x-ray measurements.

2. Neoclassical Currents

The Pfirsch-Schlüter and bootstrap currents in HSX have unique properties because of the high effective transform and the lack of toroidal curvature. The Pfirsch-Schlüter current in HSX is helical so that from the beginning of a field period to the half-way point, the dipole current reverses direction. Also, both currents are smaller than their equivalents in a tokamak which has the same real transform as in HSX. Finally, in order for the parallel current to add to the diamagnetic current so that the total current flows in the direction of symmetry, the bootstrap current in HSX flows in the opposite direction to that in a tokamak. The reversal of the bootstrap current also means that the rotational transform is reduced, rather than increased as in a tokamak. However, the transport doesn't degrade with the bootstrap current because the effective transform increases slightly.

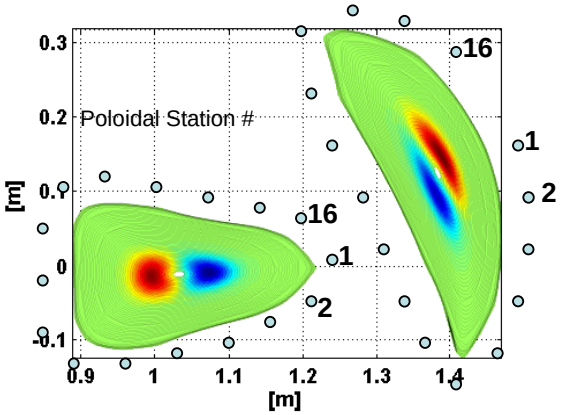

FIG. 1 Last closed magnetic surface and calculated Pfirsch-Schlüter current contours at two toroidal locations (1/6 fp on the right and 1/2 fp on the left) where the 16 3-axis magnetic coils are located, labeled 1 to 16 in the clockwise direction.

Plasma currents in HSX are measured with a set of 16 3-axis coils that measure flux in three orthogonal directions. The coils are wound on the faces of a cube and the cubes are then mounted on a nylon belt which is wrapped around the vacuum vessel and tightened into place. The location and orientation of the coils is measured. The belt containing the set of 16 triplets was first placed at the half field period (fp) position and subsequently at the one-sixth fp location. FIG. 1 is an illustration of the helical nature of the current and the approximate locations of the 16 triplets.

To model the signals detected by the 16 coil array, the VMEC [2] code is first used to calculate the equilibrium and Pfirsch-Schlüter currents, using as input the density and electron temperature profiles measured by Thomson scattering. The output of VMEC is then input into BOOTSJ [3] to calculate the bootstrap current. The current profile from BOOTSJ is then fed back into VMEC to obtain a self-consistent equilibrium. When the calculated bootstrap current differs from the preceding iteration by less than 2%, the VMEC output is then fed into the V3FIT [4] code which calculates the components of the magnetic field due to the plasma at each of the magnetic pickup coil locations.

FIG. 2 shows the radial component of the magnetic field as a function of the poloidal station # around the vacuum vessel. It can be seen from the figure that the field at the 1/2 fp location

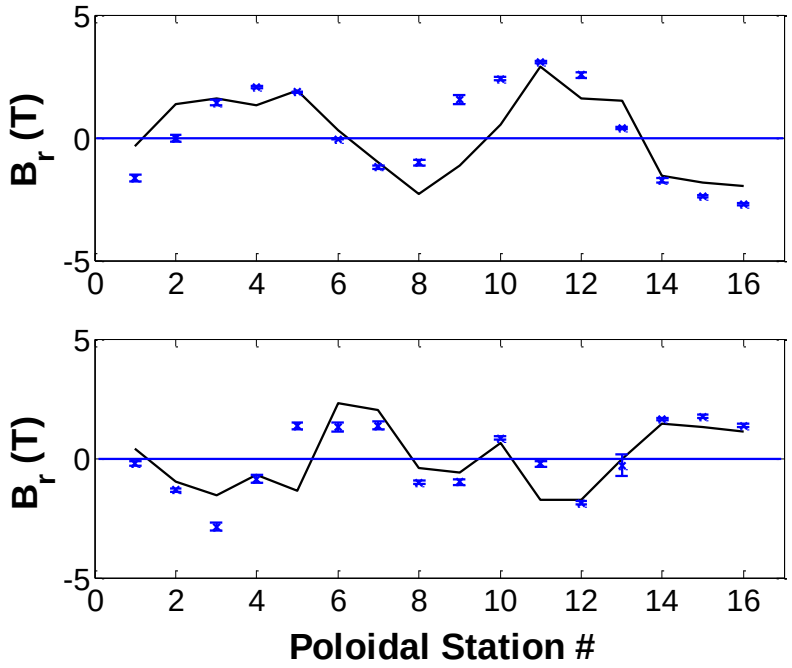

FIG. 2 Amplitude of radial magnetic field component($\times 10^{-4}$ and marked by 'x') at the 1/6 (top) and 1/2 field period (bottom) locations. Also shown are the calculated values using the V3FIT code (solid line).

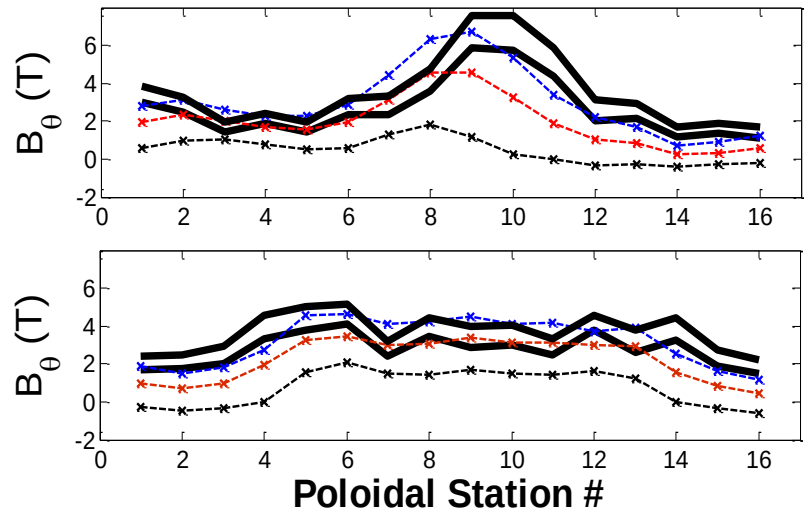

FIG. 3 Amplitude of poloidal magnetic field component ($\times 10^{-4}$ and marked by 'x') for 10, 30 and 50 ms into the discharge at the 1/6 (top) and 1/2 (bottom) fp locations. Calculated values (dark solid lines) using V3FIT are shown for t = 50 ms and for steady-state (the slightly larger value).

is almost 180^0 degrees out of phase with the signals at the 1/6 fp location. This confirms that the Pfirsch-Schlüter current in HSX is helical. FIG. 3 shows the poloidal component of the magnetic field for the two toroidal locations. The measurements, shown by the thin lines, show an increase in the poloidal field with time. This is consistent with Rogowski coil measurements which indicate that the total current in the non-ohmic plasma is increasing with time until the end of the discharge at 50 ms. The solid lines in FIG. 3 are the V3FIT calculations of the poloidal field, using an axisymmetric model to simulate the bootstrap

current evolution. Also shown in the figure is the slightly larger poloidal field calculated by V3FIT assuming the steady-state value of the bootstrap current. The measurements also confirm that the bootstrap current is indeed flowing in a direction to unwind the rotational transform and that both the Pfirsch-Schlüter and bootstrap currents are reduced compared to a tokamak, due to the high effective transform in HSX.

3. Electron Neoclassical Thermal Transport

A key element of the stellarator experimental program, as well as for optimization studies, is how to control the magnetic configuration so that anomalous transport is reduced. On LHD, for example, it has been observed that an inward shift of the plasma, which reduces neoclassical transport, also improves confinement even at high collisionalities where the contribution to transport of particles trapped in the helical ripple is negligible [5]. Theoretical models predict that lower neoclassical transport leads to larger residual zonal flows [6,7,8]. Gyrokinetic simulations demonstrate that the inward shift in LHD corresponds to a reduction in turbulent transport due to enhanced zonal flow formation, although more detailed comparison to experimental results remain [9].

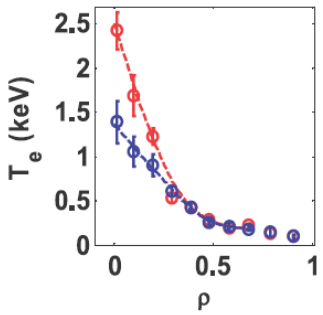

FIG. 4 Electron temperature profile for QHS (red) and Mirror (blue) for 100 kW input power.

To address how the magnetic configuration affects transport, we compare heating in QHS and Mirror at 1 Tesla. For the same 100 kW input power, FIG. 4 shows that the central electron temperature for the QHS configuration can reach 2.5 keV, while for the Mirror configuration the measured temperature was 1.5 keV. The sharp gradient in the electron temperature towards the core for the QHS configuration is indicative of an internal transport barrier and discussed further in Section 4.

By matching plasma profiles using different injected powers for the two configurations, it would be possible to compare directly the anomalous electron thermal diffusivity without having to make assumptions as to the scaling of transport with density and temperature as well as gradients. FIG. 5 shows the density and temperature profiles when 44 kW is injected into a Mirror plasma, while only 26 kW was needed for the QHS configuration. Except at r/a ~ 0, the temperature profiles agree fairly well; the density profiles differ at the plasma core.

Key to making a comparison of anomalous transport is that the neoclassical transport analysis is appropriate for a quasisymmetric stellarator. To analyze neoclassical transport for both configurations, we use the PENTA code, developed by Spong [10]. The code is based on the work of Sugama and Nishimura [11] that uses solutions to the drift kinetic equation performed by the DKES [12] code to provide transport coefficients to derive parallel components of the viscous stress tensor. Coupled to the parallel component of the momentum balance equations and the friction-flow relations and setting the ion and electron fluxes equal, the parallel flow and radial electric field can be obtained. Previously, nonsymmetric stellarators solved for the radial electric field by equating the fluxes and ignoring the parallel flow. This approximation is usually valid in configurations in which the parallel flow is strongly damped, but in quasisymmetric configurations this is not generally the case.

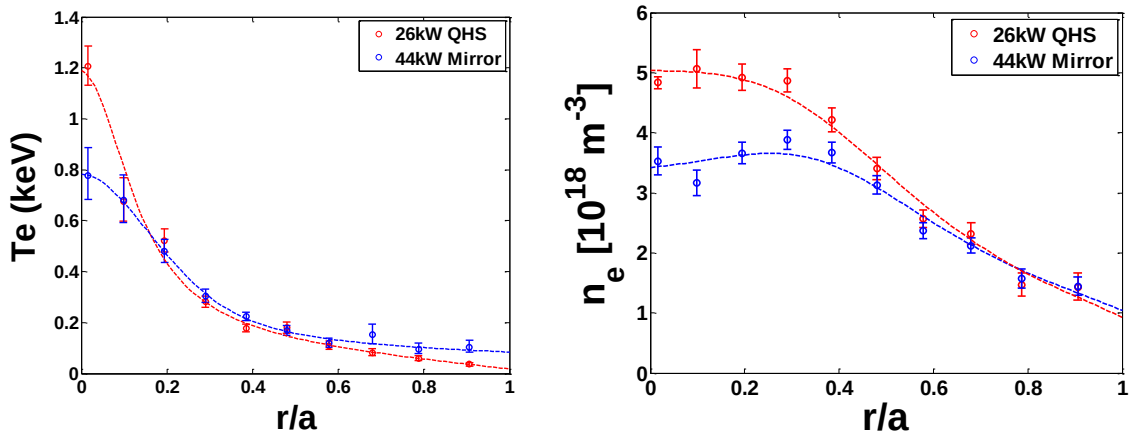

FIG. 5 Temperature and density profiles for QHS (red) and Mirror (blue) with 26 kW and 44 kW injected power respectively

FIG. 6 is a plot of the radial electric field profile for the QHS and Mirror configurations. In the core of the plasma, the electric field is large and positive, indicative of an electron root. Outside the core, the electric field is small, characteristic of an ion root. Also shown is an unstable root in the transition region. For the QHS configuration, the electric field in the core region calculated by the PENTA code is roughly half that determined by DKES without considering momentum conservation and parallel flow. For the nonsymmetric Mirror configuration, PENTA agrees well with DKES.

Experimental and neoclassical thermal conductivities are shown for the QHS and Mirror cases in FIG. 7. For the experimental conductivity, the absorbed power profile is determined by ray-tracing based on the temperature and density profiles obtained by Thomson scattering. The profile is then scaled to the total absorbed power determined from the decay of the diamagnetic loop signal during ECRH turn-off. The thermal conductivity is defined here as the total heat flux divided by the temperature gradient.

The neoclassical thermal conductivities are determined by the PENTA code. Shown in FIG. 7 are the conductivities corresponding to both the electron and the ion root. The transition

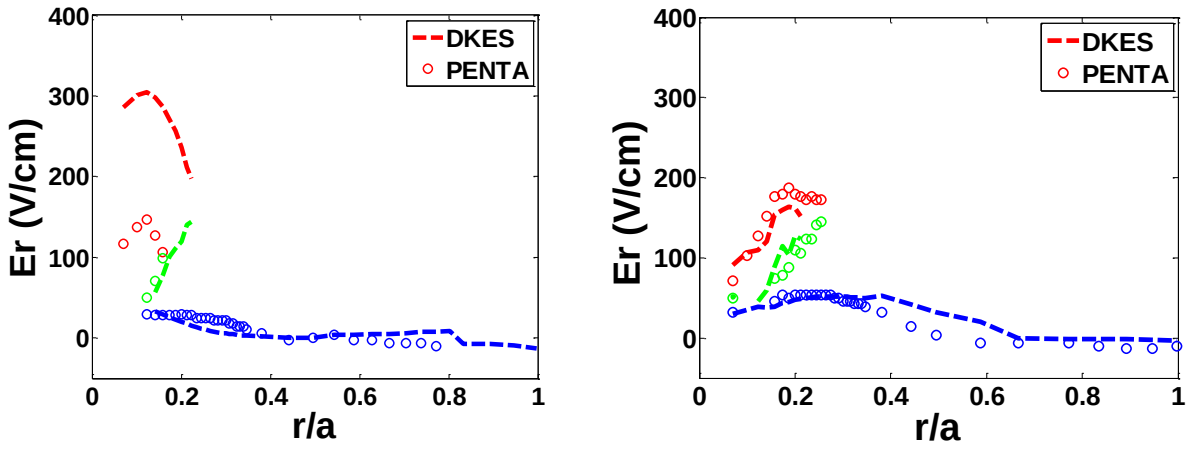

FIG. 6 Radial electric field profile for QHS (left) and Mirror (right) from DKES (lines) and PENTA (circles). Shown are the electron roots (red), ion roots (blue) and unstable roots (green).

between the roots will be the subject of future work. The difference between the experimental and neoclassical conductivities is an indication of the anomalous contribution to the transport, although the profiles are not exactly matched in the discharges under consideration here. Still, it appears that anomalous transport may be higher for the Mirror configuration. In the next section, a model for anomalous transport for HSX is discussed as well as evidence that E×B shear stabilization of turbulence due to electron/ion root proximity is responsible for the strongly peaked electron temperature profile at high power.

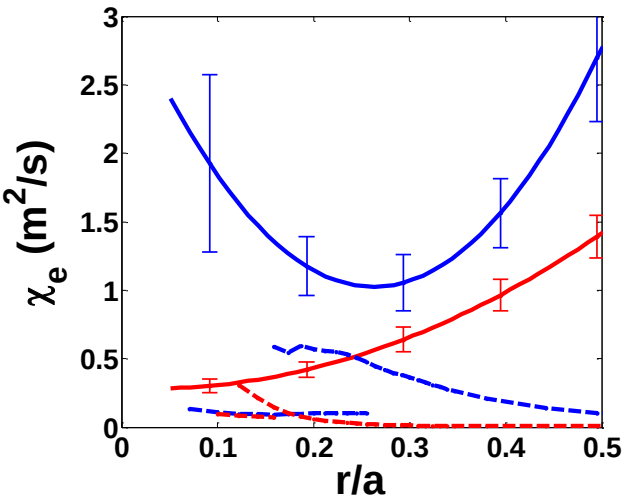

FIG. 7 Experimental (solid lines) electron thermal conductivity for QHS (red) and Mirror (blue). Also shown are the neoclassical thermal conductivities (dashed lines) for both ion and electron root solutions.

4. Anomalous Transport Modeling

The electron temperature in HSX is typically much higher than the ion temperature during ECRH so that the dominant long wavelength instability is the trapped electron mode (TEM). Because of the quasisymmetry, the magnetic geometry in HSX is similar to that in a tokamak since there is, by and large, a single class of trapped particles. To simulate anomalous transport in HSX, the Weiland model [13] for ion temperature gradient (ITG) and TEM, originally used to describe transport in tokamaks, was modified to approximate the local geometry in HSX. This required the substitution of the helical ripple in place of the toroidal ripple and a local curvature about 3 times that of a tokamak with the same major radius. The 3D gyrokinetic code GS2 [14] confirmed that the linear growth rates using the modified Weiland model were accurate to within 30 %. Details are given in the paper by Guttenfelder [15].

The very peaked electron temperature profile shown in FIG. 4 for the QHS configuration is modeled with a combination of neoclassical and anomalous transport. Two equations are solved for the evolution of the radial electric field and electron temperature,

$$\frac{\partial E_r}{\partial t} - \frac{\partial}{\partial V}\left[\langle \nabla V \rangle D_E \left(\frac{\partial E_r}{\partial r} - \frac{E_r}{r} \right)\right] = \frac{e}{\varepsilon_\perp}\left(\Gamma_e - \Gamma_i\right) \tag{3}$$

$$\frac{3}{2} n_e \frac{\partial T_e}{\partial t} - \frac{\partial}{\partial V}\left[\langle \nabla V \rangle Q_e\right] = P_{ECRH}(\rho) \tag{4}$$

where V is the volume enclosed by a flux surface, $\varepsilon_\perp = \varepsilon_0 (1+V_A^2/c^2)$ (V_A is the Alfvén velocity), D_E is the diffusion coefficient for the radial electric field, Q_e is the electron heat flux and P_{ECRH} is the power absorbed from the ECRH. The density profile is kept fixed for the simulation. FIG. 8 shows the radial electric field calculated by the standard ambipolarity constraint, which is the steady-state solution of Eq. (3) with D_E set to zero. Good agreement with the PENTA code was obtained when a value of $D_E = 0.3$ was used in Eq. (3).

FIG. 9 shows the resulting temperature profile from solving Eq (4). Outside r/a ~ 0.3, the calculated temperature agrees well with the experimental data. Inside this region, the transport predicted by the model underestimates the experimental temperature, up to a factor of two on the magnetic axis. The proximity of the electron root to the ion root suggests that the large E×B shear might be suppressing the turbulence. Gyrokinetic simulations for tokamaks [16] have shown that the reduction of turbulence can be modeled by multiplying anomalous diffusivities by a scale factor of max $(1 - \alpha_E \gamma_E/\gamma_{max}, 0)$ where α_E is on the order of 0.5, γ_E is the E×B shearing rate, and γ_{Max} is the maximum linear growth rate without shear.

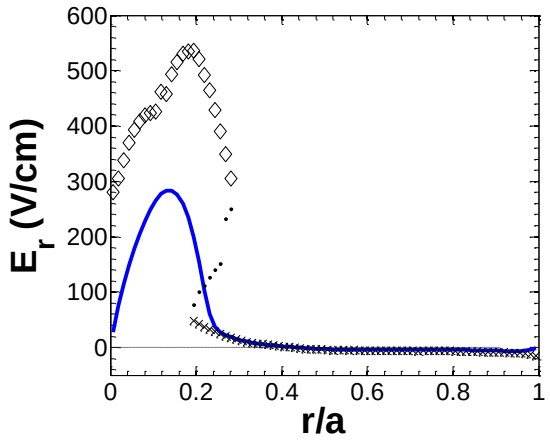

FIG. 8 The steady-state radial electric field from DKES using Eq. (3) with D_E = 0 (◊ electron root; ●unstable root; x ion root) . The blue solid curve is Eq. (3) with D_E = 0.3 to reproduce the PENTA calculations.

FIG. 9 shows that including the effects of shear suppression with a value of α_E of 0.27, the experimental profile is approximately reproduced. The simulation indicates that the shear produced by the proximity of the electron and ion root in the plasma is reducing turbulent transport, allowing for a sharply peaked electron temperature profile in the core. This strongly peaked profile has been observed on other stellarators and the improved confinement regime has been termed core electron-root confinement (CERC) [17]. Finally, FIG. 10 shows that a comparison of the electron energy confinement time τ_E for four different simulations ranging from 26 kW to 100 kW agrees well with the experimental value.

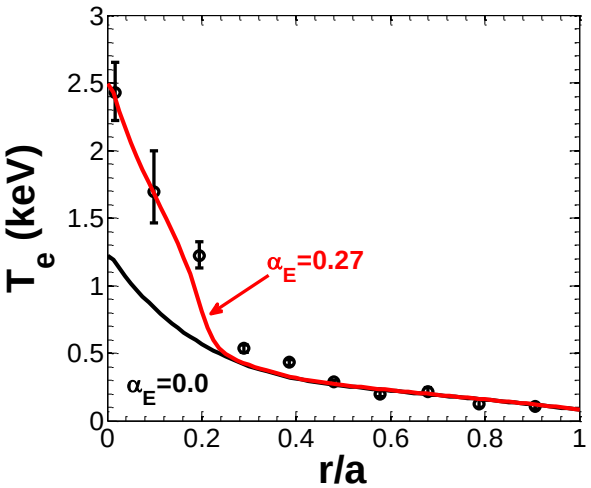

FIG. 9 Experimental electron temperature profile (●) and calculated values from Eq. (4) without shear stabilization (α_E = 0.) and with (α_E = 0.27).

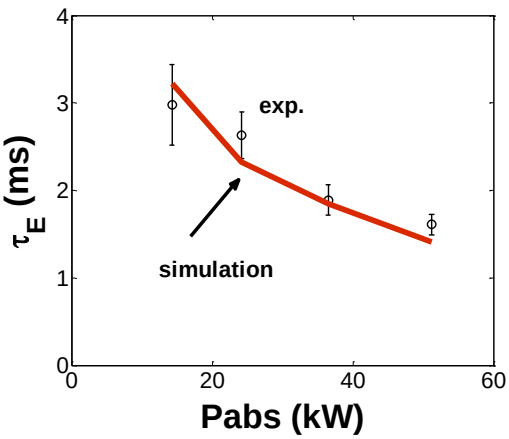

FIG. 10 Simulated and experimental confinement times for 4 different absorbed powers.

5. Discussion and Summary

Measurements of the bootstrap and Pfirsch-Schlüter currents in HSX verify the high effective transform and lack of toroidal curvature in HSX. These results confirm previous conclusions

that were based on the measurement of passing particle orbits using an electron gun and a fluorescent mesh [18]. The peak radial electric field calculated using the PENTA code for the QHS configuration was only 150 V/cm, compared to 300 V/cm obtained with DKES which ignores momentum conservation and parallel flow. These calculations will be compared to forthcoming measurements of the electric field using Charge Exchange Recombination Spectroscopy (CHERS). With up to 100 kW input power, T_e (0) ~ 2.5 keV and a very steep gradient was measured for a QHS plasma. A modified Weiland model was used to simulate anomalous transport in HSX and agreed well with gyrokinetic calculations. The Weiland model plus neoclassical transport was used to estimate the electron temperature profile during ECRH. Good agreement with the data was obtained for r/a > 0.3, but the model significantly underestimated the central electron temperature by a factor of two. Shear stabilization of turbulence due to the proximity of the electron root to the ion root solution to the ambipolarity constraint was needed to explain the high central temperature. However, gyrokinetic calculations with E×B shear are needed to better understand this phenomenon and what value α_E might be in HSX. The enhanced confinement regime, known as a CERC, has been observed in other stellarators but has now been observed for the first time in a quasisymmetric stellarator. The experimental scaling of the confinement time with power agreed well with the transport model. There is some indication that anomalous transport may be smaller in the QHS configuration compared to the Mirror. Nonlinear turbulence simulations are needed to better understand the role of zonal flows in HSX.

Acknowledgments

The authors thank D.A. Spong for the PENTA code and numerous helpful discussions. We also thank S.F. Knowlton and J.D. Hanson for help with the V3FIT code. This work was supported by the U.S. Department of Energy.

References

[1] CANIK, J.M., et. al., Phys. Rev. Lett. **98** (2007) 085002.
[2] HIRSHMAN, S.P., Comput. Phys. Commun. **43** (1986) 143.
[3] SHAING, K.C., et. al., Phys. Fluids **B1** (1989) 1663.
[4] HIRSHMAN, S.P., LAZARUS, E.A., HANSON, J.D., KNOWLTON, S.F., LAO, L.L., Phys. Plasmas **11** (2004) 595.
[5] MOTOJIMA, O., et. al., Nucl. Fusion **43** (2003) 1674.
[6] SHAING, K.C., Phys. Plasmas **12** (2005) 082508.
[7] SUGAMA, H., WATANABE, T.-H., Phys. Rev. Lett. **94** (2005) 115001.
[8] MYNICK, H.E., BOOZER, A.H., Phys. Plasmas **14** (2007) 072507.
[9] WATANABE, T.-H., SUGAMA, H., FERRANDO-MARGALET, S., Phys. Rev. Lett. **100** (2008) 195002.
[10] SPONG, D.A., Phys. Plasmas **12** (2005) 056114.
[11] SUGAMA, H., NISHIMURA, S., Phys. Plasmas **9** (2002) 4637.
[12] VAN RIJ, W.I., HIRSHMAN, S. P., Phys. Fluids **B1** (1989) 563.
[13] NORDMAN, H., et al., Nucl. Fusion **30** (1990) 983.
[14] KOTSCHENREUTHER, M., et al., Comp. Phys. Comm. **88** (1995) 128.
[15] GUTTENFELDER, W., et al., Phys. Rev. Lett., submitted.
[16] KINSEY, J.E., et al., Phys. Plasmas **12** (2005) 062302.
[17] YOKOYAMA, M., et. al., Nucl. Fusion **47** (2007) 1213.
[18] TALMADGE, J.N., et. al., Phys. Plasmas **8** (2001) 5165.